J. Phys. B: At. Mol. Opt. Phys. **41** (2008) 095703 (9pp) doi:10.1088/0953-4075/41/9/095703

Stark effect of high-*n* hydrogen-like transitions: quasi-contiguous approximation

Evgeny Stambulchik and Yitzhak Maron

Faculty of Physics, Weizmann Institute of Science, Rehovot 76100, Israel

E-mail: Evgeny.Stambulchik@weizmann.ac.il

Received 13 December 2007, in final form 4 March 2008
Published 23 April 2008
Online at stacks.iop.org/JPhysB/41/095703

Abstract

Calculations of line shapes of highly excited (Rydberg) atoms and ions are important for many topics in plasma physics and astrophysics. However, the Stark broadening of the radiative transitions originating from high-n levels of hydrogen or hydrogen-like ions is rather complex, making the detailed calculations of their spectral structure very cumbersome. Here, we suggest a simple analytical method for an approximate calculation of such line shapes. The utility of the method is demonstrated in application to the line broadening in plasma, where a very good accuracy is achieved over a range of transitions, species and plasma parameters. Although the method is especially suitable for transitions with $\Delta n \gg 1$, it describes rather well even first members of the spectroscopic series with Δn as low as 2. Accurate computer simulations are used to verify the validity of the method.

(Some figures in this article are in colour only in the electronic version)

1. Introduction

The Stark broadening of transitions involving Rydberg states is used for diagnostics of laboratory and space plasmas. Density measurements in tokamak [1–3], pinch [4], and laser-produced [5] plasmas, high-pressure arc discharges [6], flames [7], stellar atmospheres [8] and solar prominences [9] are examples of such studies. However, radiative transitions originating from high-n levels of hydrogen or hydrogen-like ions have a complex structure of the Stark effect, which poses a few calculational challenges. While effective and accurate methods for evaluating the atomic transition matrix elements are now readily available [10], the complexity due to the large number of different atomic states involved in such a transition remains an impeding factor in applying computer simulation methods employing directly solving the time-dependent Schrödinger equation for Stark broadening of high-n transitions in plasmas. The fast growth of the computational requirements with n makes such calculations unfeasible for, say $n \gtrsim 20$, using present personal computers.

For a group of degenerate levels with the principal quantum number (PQN) n, the number of distinct Stark sublevels is $2n - 1$. Therefore, a transition between n and n' has, in general, $(2n - 1)(2n' - 1)$ components (though, in the dipole approximation, several may have the same energy and/or zero intensity due to the selection rules). For transitions with high n, but relatively small $\Delta n = n - n' \ll n$, it was found [11] that the expressions for the intensities of the components can be simplified by aggregating the components into a few (of the order of Δn) groups of transitions, with the intensity distributions within each of such groups approximated analytically. This approach, therefore, allows for faster Stark broadening calculations [12, 13] which are in particular useful for a small Δn (say $\ll$10).

If $n \gg n'$, the Stark effect of the lower levels can be neglected. The number of distinct transition components is then $2n - 1$, which is still very large for high n. Among these $2n - 1$ components, the central (unshifted) one is of a special importance in the Stark broadening calculations. In the electric-dipole approximation, and neglecting the second- and higher-order corrections, its shift is exactly zero, while its intensity may be either finite or, if the PQN of the upper and the lower levels differ by an even number, exactly zero. Accordingly, the line shapes of hydrogen-like transitions with and without the central component tend to be quite different for the first members of the Lyman, Balmer and Paschen series.

However, as n goes higher, the relative intensity of the central component when it is present, or the relative intensity decrease at the line centre in its absence, becomes smaller. At the same time, the relative 'density' of the components (i.e., the number of distinct components per typical linewidth) becomes larger. Therefore, when there is a broadening mechanism (e.g., the Doppler effect or the electron-impact broadening) that exceeds the splitting between the adjacent static components, the entire line profile can be accurately described as a contiguous one, even for a constant value of the quasistatic micro-field. This 'quasi-contiguous' (QC) line shape can further be convolved with an appropriate distribution of the micro-fields in order to obtain the line shape in the quasistatic approximation. Furthermore, it will be shown that, within this approach, the dynamics of the electric fields and correlation effects in plasma can be accounted for in a simple semi-empirical way, thus providing a straightforward method for calculating Stark broadening in plasma; such calculations in many practical cases can be fully analytical.

2. The method

2.1. Static effect

Let us first consider a high-n Lyman transition. In the presence of a static, uniform electric field F, neglecting any deviation from the linear Stark effect, the upper level (and hence the spectral line) is split into $2n-1$ equispaced components (see, e.g., [14]):

$$\Delta E_{n_1 n_2 m} = \frac{3}{2} n (n_1 - n_2) \frac{e a_0}{Z} F, \tag{1}$$

where n_1, n_2 and m are the parabolic quantum numbers, satisfying the

$$n = n_1 + n_2 + |m| + 1 \tag{2}$$

condition, e is the electron charge, a_0 is the Bohr radius and Z is the core charge of the radiator (in units of $|e|$). In the dipole approximation, the relative intensity of a given component, averaged over all directions of observation, is proportional to the square of the respective radius-vector matrix element:

$$I_{n_1 n_2 m} = C |\langle 0 | \vec{r} | n_1 n_2 m \rangle|^2, \tag{3}$$

where $|0\rangle$ denotes, for brevity, the ground state and C is a proportionality factor (unimportant here). Because of the selection rules, only transitions originating from the states with $m = 0$ (π-transitions) and $m = \pm 1$ (σ-transitions) are allowed. Noticing that $|\langle 0|x|n_1 n_2 \pm 1\rangle| = |\langle 0|y|n_1 n_2 \pm 1\rangle|$, $|\langle 0|x|n_1 n_2 1\rangle| = |\langle 0|x|n_1 n_2 - 1\rangle|$, and $|\langle 0|x|n_1 n_2 0\rangle| = |\langle 0|z|n_1 n_2 \pm 1\rangle| = 0$, equation (3) can be re-written for the π and σ components separately, namely:

$$I^{(\pi)}_{n_1 n_2} = C |\langle 0|z|n_1 n_2 0\rangle|^2, \tag{4a}$$

$$I^{(\sigma)}_{n_1 n_2} = 4C |\langle 0|x|n_1 n_2 1\rangle|^2. \tag{4b}$$

Inserting the actual expressions for the matrix elements (see, e.g., equations (65.4) of [14]), we obtain

$$I^{(\pi)}_{n_1 n_2} = C^* (n_1 - n_2)^2, \tag{5a}$$

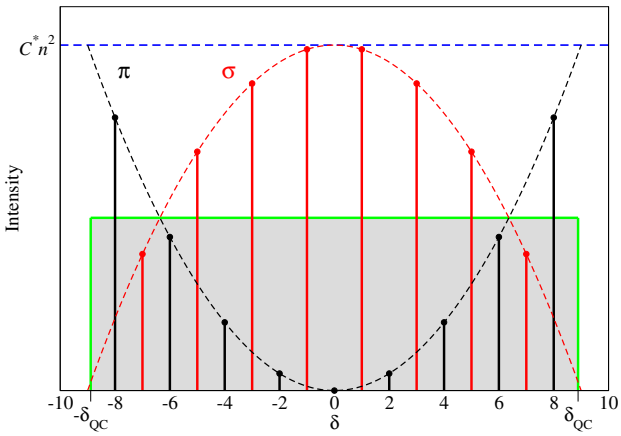

Figure 1. Static Stark effect of the Lyman $n = 9$ line. Intensities of the π and σ components form two parabolae, that, on average, can be substituted with a simple rectangular shape.

$$I^{(\sigma)}_{n_1 n_2} = 4C^* (n_1 + 1)(n_2 + 1), \tag{5b}$$

where C^* is a complex numeric factor that depends only on n and is common to both the $\langle |x| \rangle$ and $\langle |z| \rangle$ matrix elements. Substituting $n_1 - n_2$ by δ (sometimes called the 'electric quantum number') and noticing that for $|m| = 1$ (σ transitions), $(n_1 + 1)(n_2 + 1) \equiv \frac{1}{4}(n^2 - \delta^2)$ (see equation (2)), we finally obtain:

$$I_\delta = \begin{cases} C^* \delta^2, & \delta = -(n-1), -(n-3), \ldots, (n-1), \\ C^* (n^2 - \delta^2), & \delta = -(n-2), -(n-4), \ldots, (n-2). \end{cases} \tag{6}$$

On the other hand, according to equation (1), δ uniquely determines the shift of a Stark component. For $n \gg 1$, we can neglect the displacement offsets between the interleaving π and σ components and simply sum up the two branches of equation (6), which gives that the total line intensity distribution is constant over a symmetric range of the allowed values of δ, from $-\delta_{QC}$ to δ_{QC}. This is demonstrated in figure 1, where a static Stark splitting of the Lyman $n = 9$ transition is shown. In order to define the value of δ_{QC}, we let the height of the resulting QC rectangle be half of the height of the parabolic envelopes in equations (6), i.e., it is $C^* n^2/2$ (see figure 1). Since the total intensity of the line is $C^* n (n^2 - 1)$, then, in order to preserve the line intensity, one must assign

$$\delta_{QC} = n - \frac{1}{n}. \tag{7}$$

Following the discussion above, it is therefore possible to represent a static high-n Lyman QC profile (relative to the zero-field line position) as

$$I_n(\omega) = \begin{cases} \dfrac{I^{(0)}_n}{2\alpha_n F/\hbar} & \text{for} \quad |\hbar\omega| \leqslant \alpha_n F \\ 0 & \text{for} \quad |\hbar\omega| > \alpha_n F, \end{cases} \tag{8}$$

where $I^{(0)}_n$ is the total line intensity, and α_n is the linear-Stark-effect coefficient:

$$\alpha_n = \frac{3}{2}(n^2 - 1)\frac{e a_0}{Z}. \tag{9}$$

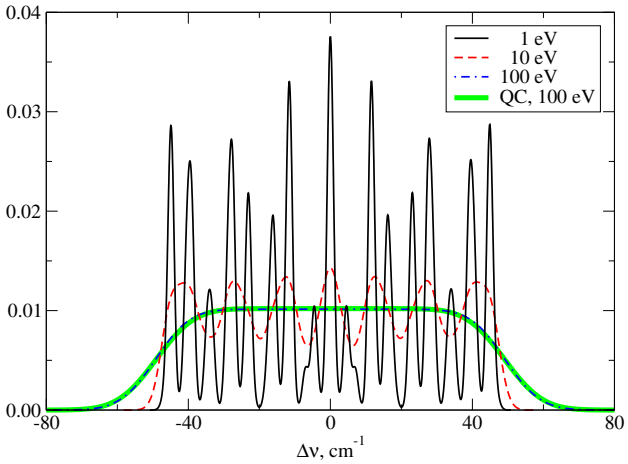

Figure 2. Linear static Stark effect of the Balmer $n = 9$ line, calculated for $F = 10$ kV cm^{-1}. Doppler broadening for different temperatures of the radiator (shown in the legend) is assumed. Also shown is the QC line shape calculated for a temperature of 100 eV. The line shapes are area normalized.

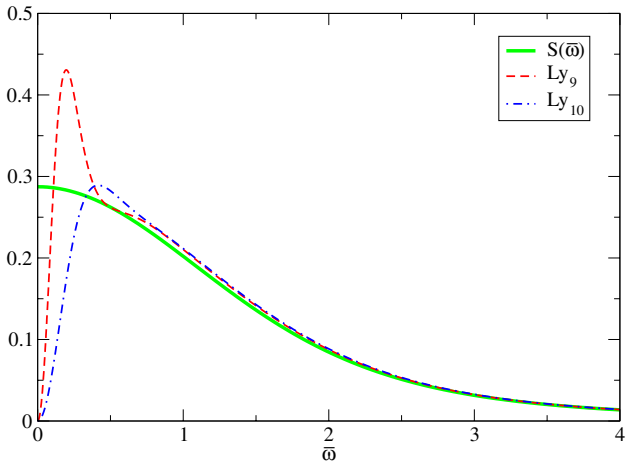

Figure 3. Quasistatic Stark effect of the Lyman $n = 9$ and $n = 10$ lines (the central component of the Ly_{10} line, which is a δ-function in the non-quenching quasistatic approximation, is not shown). The accurately calculated line shapes are compared to the QC approximation.

Although the derivation above was made for transitions from the high-n states to the ground state (the Lyman series), it is readily generalized to other transitions between levels with the principal quantum numbers n and n' by using, instead of α_n,

$$\alpha_{nn'} = \frac{3}{2}(n^2 - n'^2)\frac{ea_0}{Z}. \tag{10}$$

Evidently, for the QC approach to be applicable, the number of groups of components of such a transition must be sufficiently large, i.e., $n - n' \gg 1$.

As an example, consider the H Balmer $n = 9$ transition. In figure 2, a static-Stark-splitting pattern is convolved with several Gaussians corresponding to different Doppler temperatures T_D (convolutions with Lorentzian or Voigt profiles produce similar results). What seems to be a rather complex pattern gradually becomes a simple rectangle (convolved with the respective Gaussian). For comparison, the QC line shape, convolved with the 100 eV Gaussian, is also given in the figure, and, as seen, it is almost indistinguishable from the respective accurate calculation. We note that the specific conditions assumed in this example may not have a sound physical importance, and were selected for the sole purpose of demonstrating the equivalence of the static Stark profile to the rectangular QC shape, provided a sufficient broadening mechanism exists.

2.2. *The quasistatic approximation*

We now proceed to evaluating the line shape in the quasistatic approximation. Convolution of equation (8) with a distribution of the field magnitudes $W(F)$ gives

$$I(\omega) = \int_{\hbar\omega/\alpha_{nn'}}^{\infty} \frac{W(F)\,\mathrm{d}F}{2\alpha_{nn'}F/\hbar}, \tag{11}$$

or, using the reduced field strength $\beta = F/F_0$ and the reduced detuning $\bar{\omega} = \hbar\omega/\alpha_{nn'}F_0$,

$$I(\bar{\omega}) = \frac{1}{2}\int_{\beta}^{\infty} \frac{\bar{W}(\beta)}{\beta}\,\mathrm{d}\beta, \tag{12}$$

where

$$\bar{W}(\beta) = W(F)F_0 \tag{13}$$

and F_0 is the Holtsmark normal field strength [15]:

$$F_0 = 2\pi\left(\frac{4}{15}\right)^{2/3} Z_p e N_p^{2/3}. \tag{14}$$

Here, Z_p and N_p are, respectively, the charge and the density of the perturber particles. In the limit of the ideal plasma (i.e., with omission of particle screening and other correlations effects), the distribution function $\bar{W}(\beta)$ becomes the Holtsmark function $H(\beta)$ [15]:

$$H(\beta) = \frac{2}{\pi}\beta\int_0^{\infty} x\sin(\beta x)\exp(-x^{3/2})\,\mathrm{d}x. \tag{15}$$

In this case, the line shape according to equation (12) is merely

$$I(\bar{\omega}) = S(\bar{\omega}), \tag{16}$$

where the S function is analytically defined as

$$S(\beta) = \frac{1}{\pi}\int_0^{\infty} \cos(\beta x)\exp(-x^{3/2})\,\mathrm{d}x. \tag{17}$$

It is easy to see that $S(\beta)$ is symmetric, parabolic around $\beta = 0$, and scales as $\propto |\beta|^{-5/2}$ for $|\beta| \gg 1$. Some properties of $S(\beta)$ are given in the appendix.

As an example, we apply equations (16) and (17) to evaluations of the QC line shapes of Ly_9 and Ly_{10}. In figure 3, the computed line shapes (which, in the $\bar{\omega}$-scale, are just the S function) are compared to those computed accurately in the quasistatic approximation (an ideal plasma with the Holtsmark distribution of the field magnitudes was assumed).

As one can see, the agreement is very good for $\bar{\omega} \gtrsim 0.5$, and becomes excellent at half-width at half-maximum (HWHM) of the S curve and farther away from the line centre ($\bar{\omega} \gtrsim 1.5$). We also note that the shapes of Ly_9 and Ly_{10} are practically indistinguishable except for a rather narrow central region.

2.3. Dynamical effects

The line broadening in plasma can be correctly described in the quasistatic approximation only in rare cases. While the quasistatic approximation does work very well for the broadening caused by the ions (the ion dynamical effects, often important for hydrogen transitions with $\Delta n \sim 1$, tend to be negligible [16] for the high-n transitions discussed here), the electron contribution to the linewidth should usually be considered beyond this approximation. The validity criterion for the quasistatic approximation is that Stark shifts caused by a perturber are larger than the inverse duration of the corresponding perturber–radiator collision. For a spectral line profile as a whole, the criterion can be expressed quantitatively using a ratio between the quasistatic Stark full-width at half-maximum (FWHM) and the typical frequency of the micro-field fluctuations, i.e.,

$$R = \frac{w_{\rm qs}}{w_{\rm dyn}}. \tag{18}$$

Then, $R \gg 1$ corresponds to the quasistatic limit, while $R \ll 1$ means the impact approximation is applicable.

The quasistatic width $w_{\rm qs}$ is

$$w_{\rm qs} = 2\bar{\omega}_{1/2}\alpha_{nn'}F_0/\hbar, \tag{19}$$

where $\bar{\omega}_{1/2}$ is the HWHM width of the QC line shape. Following equation (12), $\bar{\omega}_{1/2}$ is defined implicitly by the following equation:

$$\int_0^{\bar{\omega}_{1/2}} \frac{\bar{W}(\beta)}{\beta}\,{\rm d}\beta = \int_{\bar{\omega}_{1/2}}^{\infty} \frac{\bar{W}(\beta)}{\beta}\,{\rm d}\beta. \tag{20}$$

In particular, for an ideal plasma, with the Holtsmark micro-field distribution $H(\beta)$, $\bar{\omega}^0_{1/2} \approx 1.44$. In the general case, it is convenient to factorize

$$\bar{\omega}_{1/2} = \bar{\omega}^0_{1/2}\eta_{\rm qs}, \tag{21}$$

where $\eta_{\rm qs}$ stands for corrections to the micro-field distribution function due to the correlations between the plasma particles. $\eta_{\rm qs}$ is a function of the particle densities, charges and temperature(s) in the plasma; it approaches unity in weakly coupled plasmas.

The dynamic width $w_{\rm dyn}$ in equation (18) can be estimated by the ratio between the mean relative velocity and the mean distance to the perturbers, namely:

$$w_{\rm dyn} = \frac{\langle v\rangle}{\langle r\rangle}. \tag{22}$$

Substituting $\langle v\rangle$ for the relative thermal velocity and $\langle r\rangle$ for the mean inter-particle distance of the perturbers, and introducing $\eta_{\rm dyn}$ similarly to $\eta_{\rm qs}$ in equation (21) to account for corrections due to the correlations between the plasma particles, we obtain

$$w_{\rm dyn} = \sqrt{\frac{kT_p}{m_p} + \frac{kT_r}{m_r}}\left(\frac{4\pi}{3}N_p\right)^{1/3}\eta_{\rm dyn}. \tag{23}$$

Here, T_p and T_r are, respectively, the temperatures of the perturber and the radiator species, and m_p and m_r are their masses.

After simple arithmetic transformations we obtain

$$R = 2\bar{\omega}^0_{1/2}\left(\frac{6\pi}{5}\right)^{2/3}\frac{Z_p(n^2-n'^2)}{Z} \times \frac{\hbar N_p^{1/3}}{m_e}\sqrt{\frac{m_p m_r}{k(m_rT_p + m_pT_r)}}\frac{\eta_{\rm qs}}{\eta_{\rm dyn}}. \tag{24}$$

Instead of using R, it is convenient to introduce a 'quasistaticity' factor f, defined as

$$f = \frac{R}{R + R_0}, \tag{25}$$

where R_0 is a constant of the order of unity to be determined below. The full Stark width is then

$$w = f w_{\rm qs} \tag{26}$$

(compare, e.g., with similar considerations in [13]). The meaning of the so-defined R_0 is now evident: it is a threshold determining the transition to the quasistatic limit. Indeed, for $R \gg R_0$, $f \to 1$ and $w \to w_{\rm qs}$, recovering the quasistatic approximation. On the other hand, for $R \ll R_0$, assuming for simplicity $T_p = T_r = T$, one obtains

$$w \simeq \frac{R}{R_0}w_{\rm qs} \propto \frac{Z_p^2(n^2-n'^2)^2}{Z^2}\frac{N_p}{\sqrt{T}}\frac{\eta_{\rm qs}^2}{\eta_{\rm dyn}}. \tag{27}$$

We note that the leading dependences on all the atomic and plasma parameters are *exactly* as those of the impact approximation (compare with, e.g., equation (109) of [17]). Therefore, this could in principle be used to derive the value of R_0. However, the applicability of the present method, based on the QC approximation (equation (8)), should evidently be questioned if w becomes less than the distance between the adjacent components, i.e., for $f \lesssim 1/\Delta n$. In practice, $R_0 = 0.5$ provides rather good results, as will be demonstrated in section 4.

2.4. Correlations effects

Except for the cases of strongly coupled plasmas, the plasma particle correlations are mostly restricted to pair correlations; three-body and higher-order effects are small. Therefore, the correction factors $\eta_{\rm qs}$ and $\eta_{\rm dyn}$ can be further factorized, separating the effects of the perturber–perturber (PP) and radiator–perturber (RP) interactions, namely:

$$\eta_{\rm qs} = \eta^{\rm pp}_{\rm qs}\eta^{\rm rp}_{\rm qs}, \qquad \eta_{\rm dyn} = \eta^{\rm pp}_{\rm dyn}\eta^{\rm rp}_{\rm dyn}. \tag{28}$$

The PP correlations result in the Debye screening, which evidently affects the quasistatic Stark broadening, and thus $\eta^{\rm pp}_{\rm qs}$. However, the screening is largely unimportant for the field dynamics, since neither the mean inter-particle distance nor the thermal velocities (see equation (22)) are affected by these correlations in the first order. Thus, we assume that $\eta^{\rm pp}_{\rm dyn} \approx 1$. On the other hand, the RP interactions influence both the static and dynamic properties of the micro-fields. We further argue that the ratio of the respective correction factors, $\eta^{\rm rp}_{\rm qs}/\eta^{\rm rp}_{\rm dyn}$ is rather close to unity. The weak dependence of f on

R and, thus, on $\eta_{\rm qs}^{\rm rp}/\eta_{\rm dyn}^{\rm rp}$, for the practically important values of R ($R \gtrsim 1$), further justifies this simplification. Therefore, equation (24) becomes

$$R = 2\bar{\omega}_{1/2}^{0}\left(\frac{6\pi}{5}\right)^{2/3}\frac{Z_p(n^2-n'^2)}{Z} \times \frac{\hbar N_p^{1/3}}{m_e}\sqrt{\frac{m_p m_r}{k(m_r T_p + m_p T_r)}}\eta_{\rm qs}^{\rm pp}. \quad (29)$$

If only two-particle correlation effects are retained, $\eta_{\rm qs}^{\rm pp}$ is only a function of $\langle r\rangle/\lambda_{\rm D}$, where

$$\lambda_{\rm D} = \sqrt{\frac{kT_p}{4\pi N_p e^2 Z_p^2}} \quad (30)$$

is the Debye length. To a reasonable accuracy, in weakly or moderately-coupled plasmas $\eta_{\rm qs}^{\rm pp}$ can be estimated by the Debye screening of the field of a perturber placed at the mean inter-particle distance from the radiator, i.e.,

$$\eta_{\rm qs}^{\rm pp} \approx (1+\langle r\rangle/\lambda_{\rm D})\mathrm{e}^{-\langle r\rangle/\lambda_{\rm D}}. \quad (31)$$

Similarly, the effect of the RP interactions can be estimated by

$$\eta_{\rm qs}^{\rm rp} \approx \mathrm{e}^{-r_m/\langle r\rangle}, \quad (32)$$

where

$$r_m = \frac{ZZ_p e^2}{kT_p} \quad (33)$$

is the classical distance of the minimum approach.

2.5. Multicomponent plasmas

For the calculations of line broadening in plasmas, the effect of both electrons and (a few types of) ions need to be considered simultaneously. In the general case, the total linewidth can be approximated (cf equation (26)) by the following expression:

$$w_{\rm tot} = \left[\sum_s \left(f^{(s)}w_{\rm qs}^{(s)}\right)^{3/2}\right]^{2/3}, \quad (34)$$

where the index s runs over all the plasma particle species. The expression given above is exact if the density dependence of each of the partial widths $f^{(s)}w_{\rm qs}^{(s)}$ is proportional to $N_s^{2/3}$, where N_s is the particle density of species s. This is evidently the case in the quasistatic limit, i.e., when $f^{(s)} \approx 1$. If one of the contributions departs strongly from the quasistatic limit (i.e., $f^{(s)} \ll 1$), equation (34) is, strictly speaking, no longer correct. However, the relative error is rather small, since the corresponding width $f^{(s)}w_{\rm qs}^{(s)}$ is small compared to other (quasistatic) contributions.

3. Accuracy and applicability

Let us review the accuracy of the present method. The precision of the QC line shapes in the quasistatic approximation is rather high. Indeed, except for the narrow central region (characterized by the deviation from the line centre $\Delta\omega \lesssim \mathrm{HWHM}/\Delta n$), the line shape is evaluated accurately. The only approximation used, a neglect of the relative shifts of the interleaving π and σ components (see equation (6)), results in a relative error of the order of $O(1/(\Delta n)^2)$. Furthermore, the central region of the line shape can also be described accurately provided that there exists another broadening mechanism (either a genuine physical one like, e.g., the Doppler effect, or an instrumental broadening) that contributes $\gtrsim \mathrm{HWHM}/\Delta n$ to the total line width.

Evidently, the accuracy in the quasistatic approximation (equation (12)) crucially depends on the accuracy in knowing the distribution of the micro-field magnitudes $\bar{W}(\beta)$. In the case of an ideal plasma, the analytical expression (17) is given, which, however, should not be used if the correlation effects are significant. These effects can be approximately accounted for using equations (31) and (32). Evidently, they should not be relied upon if a high accuracy is required; nor should they be used for strongly coupled plasmas, where the number of particles in the Debye sphere is $\lesssim 1$. In these cases, an accurate calculation of the micro-field distribution function $\bar{W}(\beta)$ is desired (see, e.g., [18]).

The treatment of the dynamical corrections given by equations (24)–(26) is a semi-empirical one. It is difficult to evaluate its accuracy in a rigorous way. As was mentioned at the end of section 2.3, one should require that the dynamically-narrowed (due to the f factor) line width still exceed the splitting between the adjacent static components (or groups of components, if n' is not negligibly small compared to n), i.e., $R/R_0 \gtrsim 1/\Delta n$. This can be conveniently re-written using dimensionless combinations of parameters as

$$(n^2-n'^2)(n-n')\left(N_p^{1/3}\lambda\!\!\!^{-}_e\right)\frac{Z_p}{Z}\left(\frac{m_p^*}{m_e}\right)^{1/2} \gtrsim 0.1, \quad (35)$$

where m_p^* is the reduced mass of the perturber (in the centre-of-mass frame of the radiator and the perturber), $\lambda\!\!\!^{-}_e$ is the electron de Broglie length $\hbar/(m_e kT)^{1/2}$, and, for simplicity, equal temperatures $T_p = T_r = T$ of the perturbers and the radiators were assumed. In particular, for electrons this criterion reads as

$$(n^2-n'^2)(n-n')\left(N_e^{1/3}\lambda\!\!\!^{-}_e\right)/Z \gtrsim 0.1. \quad (36)$$

For example, for a plasma with $N_e = 10^{15}$ cm^{-3} and $kT = 1$ eV, the electron broadening of the Balmer series ($n' = 2$) is described correctly by the present method starting with $n = 5$, i.e., for H_γ and above. Evidently, for ions criterion (35) is significantly weaker; e.g., the broadening of the same H_γ line due to the protons can be calculated using this method for much lower densities, $N_e \gtrsim 10^{10}$ cm^{-3}, $kT = 1$ eV.

Finally, we examine the applicability of the physical approximations used. The use of the dipole approximation is justified for electric fields that are weak enough for the higher-order-multipole corrections to remain small. An obvious criterion is that the change of the plasma electric field is small on the spatial scale of the radiator size, i.e., for each perturber species p

$$\frac{n^2}{Z}a_0 N_p^{1/3} \ll 1. \quad (37)$$

The neglect of the quenching interactions (i.e., those involving levels with different PQN), resulting in deviations from the linear Stark effect can be used when the linear Stark effect of

a given level is significantly smaller than the distance to the next neighbouring level:

$$\bar{\omega}_{1/2}\alpha_n F_0 \ll \frac{Z^2e^2}{2a_0}\left[\frac{1}{n^2}-\frac{1}{(n+1)^2}\right]\approx\frac{Z^2e^2}{a_0n^3}. \qquad (38)$$

This can be conveniently re-written as

$$5.6\eta_{\rm qs}\frac{Z_p n^5}{Z^3}a_0^2N_p^{2/3}\ll 1. \qquad (39)$$

Criteria (37) and (39) are derived assuming a typical micro-field magnitude. However, the quasistatic QC line shape (equation (12)) is a convolution that also includes much stronger fields ($\beta \gg 1$). Nevertheless, the fields that determine the line width are moderate ($\beta \sim 1$), since the low probability of the strong fields make them unimportant.

The last issue that needs to be considered is whether the inelastic collisions are important. This is relevant for high-n transitions, however, with rather small $n - n' \sim 1$, for example, the high-n radio recombination lines. Here, the smallness of $n-n'$, and thus of all non-quenching contributions to the line width, makes the broadening due to the inelastic collisions with plasma particles relatively large (or even dominant) [19].

4. Examples of calculations

We compare results of the present method with those of a computer simulation modelling (CSM) [20], applied to three different cases. In the examples, thermal equilibrium was always assumed, i.e., the temperatures of all plasma species were set equal. The only free parameter of the present method, R_0, was assumed to be 0.5 in *all* examples. In addition, in order to examine the sensitivity of the method to the choice of this parameter, the calculations were repeated for $R_0 = 0.25$ and 1.0.

The first set of calculations was performed for the Balmer lines of hydrogen in a plasma with $N_e = 1.2 \times 10^{13}$ cm^{-3}, $kT = 0.16$ eV (such plasma parameters are typical for radio-frequency discharge setups). In figure 4 the results are compared to the CSM values[1], where it is seen that the agreement is very good (all differences are less than 10%). Overall, the results are rather insensitive to a specific choice of R_0; varying it between 0.25 and 1.0 sweeps a very narrow band, designated by the hashed area in figure 4 (the other examples considered below confirm this). There, the lower boundary of the hashed area corresponds to $R_0 = 1.0$ while the upper boundary corresponds to $R_0 = 0.25$. Furthermore, while the spread in the results due to different R_0's increases with n, the *relative* uncertainty it introduces actually decreases. This is expected, since the higher n is, the better all perturbers are described by the quasistatic approximation, therefore, a specific choice of the 'quasistaticity threshold' becomes less important.

The second set of calculations was done for the Balmer lines of deuterium in a plasma with $N_e = 5 \times 10^{14}$ cm^{-3}, $kT = 4$ eV, conditions typical for magnetic fusion experiments. The results are given in figure 5. Most of the CSM calculations in this case are from [16], but in addition, the calculations were also performed for lower-n members of the series, down to H_α. The agreement with the CSM calculations is excellent (within ≈5%), starting with $\Delta n = 3$. Even for Δn as small as 2 (i.e., H_β), the accuracy is reasonable, ≈10%.

Finally, analysed were the Lyman series of neon in a deuterium plasma with $N_e = 10^{21}$ cm^{-3}, $kT = 1000$ eV (such a plasma may exist in a mega-ampere gas-puff z-pinch setup, with neon used as a dopant). The agreement in this case is also very good, <10%, see figure 6. No transitions from levels with n higher than 7 were considered, since for the plasma parameters assumed, these levels vanish because of the plasma continuum lowering.

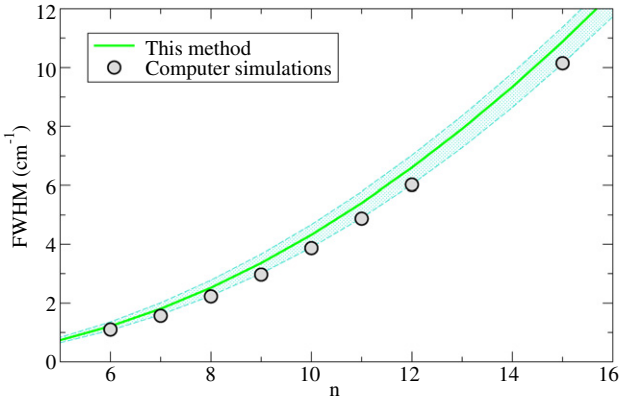

Figure 4. Stark broadening of the H Balmer transitions. $N_e = 1.2 \times 10^{13}$ cm^{-3}, $kT = 0.16$ eV. The solid line corresponds to $R_0 = 0.5$, while the hashed area designates results obtained by varying R_0 between 0.25 and 1.0 (see the text).

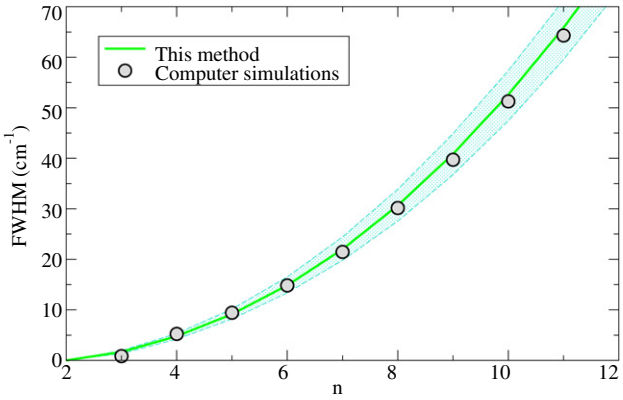

Figure 5. Stark broadening of the D Balmer transitions. $N_e = 5 \times 10^{14}$ cm^{-3}, $kT = 4$ eV.

5. Discussion

A line shape of an electric-dipole ($E1$) transition can be expressed via the autocorrelation function

$$C(t) = \mathrm{Tr}\langle\vec{D}(0)\cdot\vec{D}(t)\rangle \qquad (40)$$

[1] The details of the CSM calculations, as well as an accuracy analysis, are given in [16] (referred to as 'CSM2' there). The agreement with other calculations and, where available, with experimental data was shown to be very good.

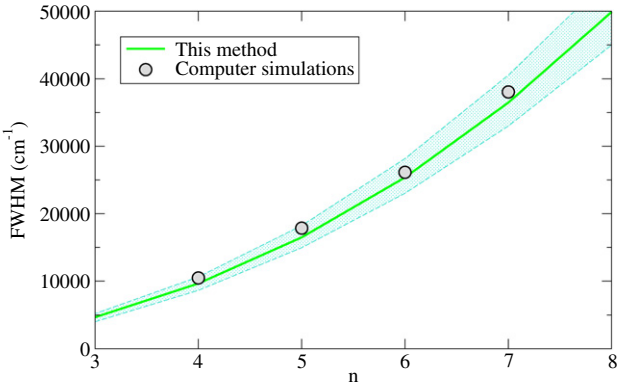

Figure 6. Stark broadening of the Ne x Lyman transitions. $N_e = 10^{21}$ cm^{-3}, $kT = 1000$ eV. Neon is assumed as a minority in the deuterium plasma.

of the dipole moment of the radiator $\vec{D}(t)$, namely [17]:

$$I(\omega) = \frac{1}{\pi} \mathrm{Re} \int_0^\infty \mathrm{d}t \exp(\mathrm{i}\omega t) C(t). \tag{41}$$

The brackets $\langle\rangle$ in equation (40) denote averaging over a statistical ensemble. Correspondingly,

$$C(t) = \int_{-\infty}^{\infty} \mathrm{d}\omega \exp(-\mathrm{i}\omega t) I(\omega). \tag{42}$$

Using equations (16) and (A.6), we obtain for the QC line shape in the ideal plasma limit:

$$C(\bar{t}) = \exp(-|\bar{t}|^{3/2}), \tag{43}$$

where, similarly to $\bar{\omega}$, the reduced time $\bar{t}$ is defined by $\bar{t} = t\alpha_{nn'}F_0/\hbar$.

Due to the large difference in the masses of electrons and ions, it is not uncommon to address situations where, simultaneously, ions are nearly quasistatic while electrons are fully in the impact regime. In such cases, the total line shape can be obtained by a convolution of the quasistatic ion contributions to the line shape with that of the electrons. The latter is a Lorentzian with the width determined by the so-called impact operator, for which an analytical expression in the dipole, non-quenching approximation (i.e., under the assumptions also used throughout the present work) has been recently made available [21]. The convolution implies that the impact operator is largely independent of the ionic field, an assumption that is often correct [22] (see, however, [23]). The total dipole autocorrelation function is a product of the ionic and electronic autocorrelation functions:

$$C(\bar{t}) = C^{(i)}(\bar{t}) C^{(e)}(\bar{t}). \tag{44}$$

In the ideal plasma limit, $C^{(i)}(\bar{t})$ is given by equation (43), thus

$$C(\bar{t}) = \exp(-|\bar{t}|^{3/2} - \bar{\gamma}|\bar{t}|), \tag{45}$$

where $\bar{\gamma}$ is the reduced (in units of $\alpha_{nn'}F_0/\hbar$) HWHM of the Lorentzian. Therefore, using equations (41) and (A.7):

$$I(\bar{\omega}) = \frac{1}{\pi} \int_0^\infty \cos(\bar{\omega}x) \exp(-\bar{\gamma}x - x^{3/2}) \,\mathrm{d}x. \tag{46}$$

We note that the asymptotic behaviour of $C(t)$ for sufficiently large $\bar{t} \gg \bar{\gamma}^2$ is $\exp(-|\bar{t}|^{3/2})$, different from the $\exp(-\bar{\gamma}|\bar{t}|)$ dependence of the impact approximation[2].

Using considerations similar to those laid out in section 2.3, one can extend the notion of the 'quasistaticity', defined by equation (25) as a mean value for an entire line shape, to be a function of the detuning ω from the unperturbed spectral line position. In the sufficiently far wings of the line, say beyond some ω_c, $f(\omega)$ approaches unity, ensuring that the quasistatic approximation holds. An estimate of the critical detuning ω_c is given (see, e.g., [16]) by

$$\omega_c = \frac{4kTm_e}{3\hbar(n^2 - n'^2)m_p^*}, \tag{47}$$

While, as was mentioned earlier, for the high-n transitions the ions are quasistatic practically over the entire line shape ($f^{(i)}(\omega) \equiv 1$), for electrons ω_c is often comparable to or exceeds the total linewidth. In this spirit, it was suggested [24] that an entire line shape can adequately be described by a quasistatic line shape, however, the effective quasistatic perturber density $N_{\mathrm{eff}} \equiv (1 + f^{(e)}(\omega))N_e$ becomes a parameter, varying from N_e ($|\omega| \ll \omega_c$) to $2N_e$ ($|\omega| \gg \omega_c$). The $f^{(e)}(\omega)$ dependence was sought in [25] in an empirical way, satisfying the $f^{(e)}(0) = 0$ and $f^{(e)}(|\omega| \gg \omega_c) \to 1$ conditions. We note that the $f^{(e)}(0) = 0$ condition implies a negligible contribution due to the electrons to the spectral region of the line core, which, however, becomes less justified for higher PQN. Indeed, it was shown [16] that the higher n, the relative contribution to the linewidth due to the electrons becomes larger. Furthermore, for high-n transitions the effect of the electrons becomes closer to the quasistatic limit, so that the N_e dependence of the total linewidth approaches $\sim N_e^{2/3}$, i.e., that of the quasistatic approximation. Therefore, we expect that $f^{(e)}(0)$ is *larger* than zero, and, as n approaches infinity, $f^{(e)}(0)$ approaches unity.

For convenience, a scaled (in the β domain) variant of $S(\beta)$ can be defined as follows:

$$S_f(\beta) \equiv f^{-2/3} S(f^{-2/3}\beta), \tag{48}$$

or, in the integral representation,

$$S_f(\beta) = \frac{1}{\pi} \int_0^\infty \cos(\beta x) \exp(-f x^{3/2}) \,\mathrm{d}x. \tag{49}$$

In particular, $S_2(\beta)$ corresponds to the Holtsmark distribution of a doubled density. Then, if the correlation effects are small, the line shape of any high-n transition can be expected to lie between the $S_1(\beta)$ and $S_2(\beta)$ curves. In the far wings, where both electrons and ions can safely be treated quasistatically, the line shape should asymptotically approach $S_2(\beta)$, and the higher n is, the closer to the line core this should happen (for the same plasma parameters).

These assumptions can be tested by looking at the computer-simulated [16] line shapes of the Balmer lines of hydrogen whose widths are given in figure 4. The line shapes are shown in figure 7 (for clarity, only the H_6, H_9, H_{12} and

[2] The latter should be expected (and, indeed, was observed in simulations) for spectral lines with a strong, well-resolved, unshifted component, such as Lyman α or Balmer α in sufficiently dilute plasmas. Treatment of such line shapes is evidently beyond the applicability of the QC approach.

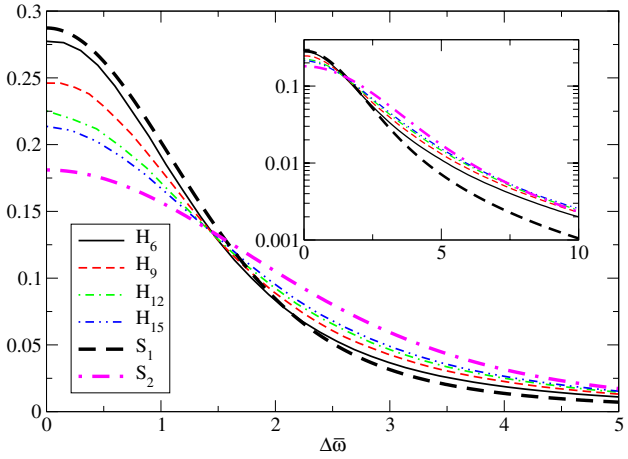

Figure 7. Stark line shapes of the Balmer H_6, H_9, H_{12}, and H_{15} transitions. The plasma parameters assumed are $N_e = 1.2 \times 10^{13}$ cm^{-3} and $kT = 0.16$ eV.

H_{15} line shapes are given). Indeed, the cores of the profiles fill in the area between the S_1 and S_2 curves, with H_6 almost matching S_1, while higher-n lines gradually shift towards S_2. Moreover, the far-wing profiles of all transitions closely approach the S_2 curve, seen clearly on the semi-logarithmic scale in the inset.

6. Conclusions

Numerical calculations of the Stark broadening of radiative transitions originating from high-n levels of hydrogen or hydrogen-like ions tend to be complicated. Here, we suggested a simple analytical method for the Stark-width calculations for such lines. The method is applicable when using the dipole approximation is sufficient. Accurate computer simulations were used to verify the validity of the method. A $\lesssim 10\%$ accuracy is achieved over a broad range of transitions, species and plasma parameters. Although for the derivation it was assumed that $\Delta n \gg 1$, even first members of the spectroscopic series with Δn as low as 2 are described very well by the method suggested.

Acknowledgments

We are indebted to S Alexiou, H R Griem, and J D Hey for their critical comments. Suggestions and comments by an anonymous referee are highly appreciated. This work was partially supported by the Minerva Foundation, with funding from the Federal German Ministry for Education and Research, and by the Israel Science Foundation (ISF).

Appendix. Some properties of $S(\beta)$

Definition

$$S(\beta) = \frac{1}{\pi}\int_0^\infty \cos(\beta x)\exp(-x^{3/2})\,\mathrm{d}x. \tag{A.1}$$

Relation to the Holtsmark function $H(\beta)$

$$\frac{\mathrm{d}S(\beta)}{\mathrm{d}\beta} = -\frac{1}{2}\frac{H(\beta)}{\beta}. \tag{A.2}$$

Peak value

$$S(0) = \frac{2}{3\pi}\Gamma\left(\frac{2}{3}\right) \approx 0.287. \tag{A.3}$$

Small-β limit

$$S(\beta) = S(0) - \frac{\beta^2}{3\pi} + O(\beta^4). \tag{A.4}$$

Large-β limit

$$S(\beta) = \frac{3}{\sqrt{32\pi}}|\beta|^{-5/2} + O(|\beta|^{-7/2}). \tag{A.5}$$

The Fourier transform

$$\begin{aligned}\bar{S}(\tau) &= \int_{-\infty}^{\infty}\mathrm{d}\beta\,\mathrm{e}^{-\mathrm{i}\beta\tau}S(\beta)\\ &= \frac{1}{2\pi}\int_{-\infty}^{\infty}\mathrm{d}\beta\int_0^\infty \mathrm{d}x[\mathrm{e}^{\mathrm{i}\beta(x-\tau)} + \mathrm{e}^{-\mathrm{i}\beta(x+\tau)}]\exp(-x^{3/2})\\ &= \int_0^\infty \mathrm{d}x[\delta(x-\tau)+\delta(x+\tau)]\exp(-x^{3/2})\\ &= \exp(-|\tau|^{3/2}).\end{aligned} \tag{A.6}$$

Convolution with (unshifted) Lorentzian $L(\beta;a) = \frac{1}{\pi}\frac{a}{\beta^2+a^2}$

$$\begin{aligned}S(\beta) * L(\beta;a) &= \frac{1}{2\pi}\int_{-\infty}^{\infty}\mathrm{d}x\,\mathrm{e}^{\mathrm{i}\beta x}\bar{S}(x)\bar{L}(x)\\ &= \frac{1}{2\pi}\int_{-\infty}^{\infty}\mathrm{d}x\,\mathrm{e}^{\mathrm{i}\beta x}\exp(-|x|^{3/2}-a|x|)\\ &= \frac{1}{\pi}\int_0^\infty \cos(\beta x)\exp(-ax-x^{3/2})\,\mathrm{d}x.\end{aligned} \tag{A.7}$$

Similarly, convolution with (unshifted) Gaussian $G(\beta;\sigma) = \frac{1}{\sqrt{2\pi}\sigma}\exp\left(-\frac{\beta^2}{2\sigma^2}\right)$

$$S(\beta) * G(\beta;\sigma) = \frac{1}{\pi}\int_0^\infty \cos(\beta x)\exp\left(-\frac{\sigma^2x^2}{2} - x^{3/2}\right)\mathrm{d}x. \tag{A.8}$$

References

[1] Welch B L, Griem H R, Terry J, Kurz C, LaBombard B, Lipschultz B, Marmar E and McCracken G 1995 Density measurements in the edge, divertor and X-point regions of Alcator C-mod from Balmer series emission *Phys. Plasmas* **2** 4246

[2] Pigarov A Yu, Terry J L and Lipschultz B 1998 Study of the discrete-to-continuum transition in a Balmer spectrum from Alcator C-mod divertor plasmas *Plasma Phys. Control. Fusion* **40** 2055–72

[3] Koubiti M, Capes H, Godbert-Mouret L, Marandet Y, Meigs A, Rosato J, Rosmej F B and Stamm R 2006 Density diagnostic using Stark broadening of He I spectral line emission from Rydberg levels *Contrib. Plasma Phys.* **46** 661–6

[4] Wong K L, Springer P T, Hammer J H, Iglesias C A, Osterheld A L, Foord M E, Bruns H C, Emig J A and Deeney C 1998 Spectroscopic characterization of an argon-neon *Z*-pinch plasma at stagnation *Phys. Rev. Lett.* **80** 2334–7

[5] Fournier K B *et al* 2003 Rydberg transitions in the spectra of near-neon-like Cu and Zn ions in different laser-produced plasmas: observations and modeling *J. Quant. Spectrosc. Radiat. Transfer* **81** 167–82
[6] Omar B, Wierling A, Günter S and Röpke G 2007 Hydrogen Balmer spectrum from a high-pressure arc discharge: revisited *Contrib. Plasma Phys.* **47** 315–23
[7] Axner O and Berglind T 1986 Stark structure observation in Rydberg states of Li in flames by laser-enhanced ionization: a new method for probing local electrical fields in flames *Appl. Spectrosc.* **40** 1224–31
[8] Hoang-Binh D, Brault P, Picart J, Tran-Minh N and Vallee O 1987 Ion-collision broadening of solar lines in the far-infrared and submillimeter spectrum *Astron. Astrophys.* **181** 134–7
[9] Chang E S and Deming D 1998 Accurate determination of electron densities in active and quiescent prominences: the mid-infrared advantage *Sol. Phys.* **179** 89–114
[10] Hey J D 2007 Some properties of Stark states of hydrogenic atoms and ions *J. Phys. B: At. Mol. Opt. Phys.* **40** 4077–96
[11] Gulyaev S A 1976 Profile of the H $n\alpha$ radio lines in a static ion field *Astron. Zh.* **53** 1010–16
[12] Bureyeva L A, Lisitsa V S and Shuvaev D A 2002 Statistical and dynamic intensities of atomic spectral lines in plasma *J. Exp. Theor. Phys.* **95** 662–72
[13] Mossé C, Calisti A, Stamm R, Talin B, Bureyeva L A and Lisitsa V S 2004 A universal approach to Rydberg spectral line shapes in plasmas *J. Phys. B: At. Mol. Opt. Phys.* **37** 1343–52
[14] Bethe H A and Salpeter E E 1977 *Quantum Mechanics of One- and Two-Electron Atoms* (New York: Plenum)
[15] Holtsmark J 1919 Über die verbreiterung von spektrallinien *Ann. Phys., Lpz.* **58** 577–630
[16] Stambulchik E, Alexiou S, Griem H R and Kepple P C 2007 Stark broadening of high principal quantum number hydrogen Balmer lines in low-density laboratory plasmas *Phys. Rev.* E **75** 016401
[17] Griem H R 1974 *Spectral Line Broadening by Plasmas* (New York: Academic)
[18] Iglesias C A, Lebowitz J and McGowan D 1983 Electric microfield distributions in strongly coupled plasmas *Phys. Rev.* A **28** 1667
[19] Griem H R 1967 Stark broadening by electron and ion impacts of $n\alpha$ hydrogen lines of large principal quantum number *Astrophys. J.* **148** 547
[20] Stambulchik E and Maron Y 2006 A study of ion-dynamics and correlation effects for spectral line broadening in plasma: K-shell lines *J. Quant. Spectrosc. Radiat. Transfer* **99** 730–49
[21] Gigosos M A, González M Á, Talin B and Calisti A 2007 Exact expression of the impact broadening operator for hydrogen Stark broadening *Astron. Astrophys.* **466** 1189–96
[22] Alexiou S 1996 Frequency separation method for relaxation problems *Phys. Rev. Lett.* **76** 1836
[23] Barbés A, Gigosos M A and González M Á 2001 Analysis of the coupling between impact and quasistatic field mechanisms in Stark broadening *J. Quant. Spectrosc. Radiat. Transfer* **68** 679–88
[24] Edmonds F N, Schlüter H and Wells D C 1967 Hydrogen-line Stark broadening functions *Mem. R. Astron. Soc.* **71** 271
[25] Schlüter H 1968 Studies on the transition from quasi-static to impact electron contributions of linear Stark broadening *J. Quant. Spectrosc. Radiat. Transfer* **8** 1217–32